Imperfection Behavior of Elastic Nonlinear Systems Illustrated by a Three-Degree-of-Freedom Model

Wibisono Hartono* and Fumio Nishino†
University of Tokyo, Tokyo, 113, Japan

A simple three-degree-of-freedom spring model system is presented to study the instability behavior of perfect and imperfect systems. The model has all known types of critical points: the stationary point and symmetric and asymmetric bifurcation points. By changing three parameters of the model, the behavior of the system can be altered and investigated. Numerical results are presented to demonstrate instability behavior of perfect and imperfect elastic nonlinear systems. Major findings are 1) an equilibrium path may terminate at a point and jump to another point even when geometric change is continuous; 2) the optimum solutions for the mode of imperfection that gives the lowest carrying capacity may also terminate at a point and jump to another point even when norms of imperfections are changed continuously; 3) an iterative process most likely diverges when the aforementioned two conditions take place unless an initial guess solution closer to the jumped position is used; 4) even for the same mode of imperfection, the load carrying capacities are not necessarily the same when norms of initial imperfections approach zero, depending on the signs of the mode; and 5) when hidden critical points are present, the structure is extremely sensitive to imperfection.

Nomenclature

e_i = unit eigenvector corresponding to ith eigenvalue
f_i, f = loading pattern vector
K_i = nondimensional equilibrium equation in x_i direction
k = spring constant
L = projected length of linear spring of perfect model
ℓ_i = nondimensional initial length of ith linear spring
$\hat{\ell}_i$ = nondimensional displaced length of ith linear spring
N_i = resisting force of ith spring
p = f/kL, nondimensional loading intensity, where f is loading intensity
r = nondimensional norm of imperfections
x_i = displaced position
x_i^0 = initial position
β = ratio between height and projected length of linear spring of perfect model
γ = given positive nondimensional constant
δ = given nondimensional constant
η_i = nondimensional displacement of ith spring
λ_i = ith eigenvalue of tangential stiffness matrix
λ_s = smallest eigenvalue of tangential stiffness matrix
χ_i = x_i/L, nondimensional displaced position
χ_i^0 = x_i^0/L, nondimensional initial position
$(\bar{\ })$ = quantities of perfect model
$(\ )^c$ = quantities at first critical point
$(\ )^{cr}$ = quantities at critical points
$(\ )^*$ = quantities at optimum first critical point

Introduction

THE study of the effect of imperfection on the carrying capacity of a structure was made on both distinct[1,2] and compound[3,4] critical points. All of them tried to derive the relation between the loading intensity and an imperfection parameter that determines the imperfection sensitivity of a system.

All these previous works on the effect of imperfection dealt with a given mode of imperfection. This given mode was either arbitrary[5,6] or a mode of the bifurcation paths at the first critical point of the main equilibrium path.[7] Nishino and Hartono[8] tried for the first time to consider the influence of modes of other critical points on imperfection behavior. They also employed an optimization process to obtain the mode of initial imperfection that gives the lowest carrying capacity of an imperfect system for a given norm of imperfections. The corresponding mode of imperfection then was defined as the critical mode of imperfection.

This paper presents a comprehensive study of the behavior of perfect and imperfect elastic nonlinear systems by analyzing numerically a simple three-degree-of-freedom model. The model is capable of exhibiting more than one bifurcation path and all known types of critical points: the stationary point and symmetric and asymmetric bifurcation points. The model has three parameters, the values of which determine the locations, existence, and disappearance of bifurcation points and the shape of its main and bifurcation paths.

This paper also presents a study to investigate the relation between the shape of equilibrium paths of a perfect system and the modes of imperfection to be used as an initial guess solution to obtain the critical mode of imperfection. The aim of this is to reduce the computational work of the optimization by proper selection of an initial guess solution.

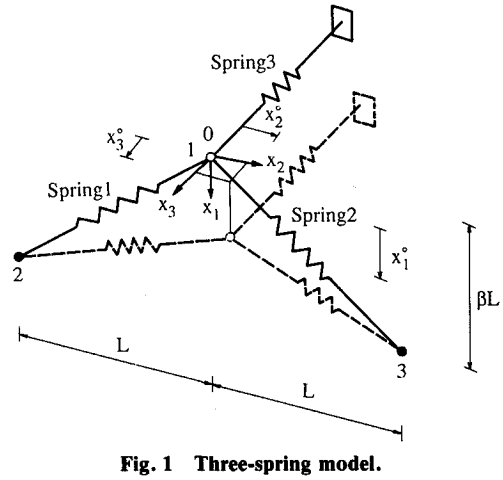

Fig. 1 Three-spring model.

Received May 23, 1989; revision received July 26, 1990; accepted for publication Aug. 23, 1990.
*Graduate Student, Department of Civil Engineering.
†Professor, Department of Civil Engineering.

Description of the Model

The model consists of three springs connected at one node in three-dimensional space. The perfect and imperfect shapes of the model used in this study are shown in Fig. 1 together with the right-handed Cartesian coordinate system with the origin 0 at the connecting node of the springs of the perfect model. The first two springs are identical linear springs that are placed on a vertical plane in perfect configuration, forming a symmetric triangle. The third spring is nonlinear and placed perpendicular to the first two. The other ends of the linear springs are fixed, while that of the third spring has a roller support that is assumed to remain parallel to its original position. These springs were selected so that the model could have stationary points on its main path and both symmetric and asymmetric bifurcation points under the application of a vertical load. It has only three degrees of freedom at the connecting node, which makes the study simple.

The resisting forces of the three springs are given as

$$\frac{N_i}{kL} = \eta_i \quad (i=1,2), \qquad \frac{N_3}{(\gamma k)L} = \eta_3 \left\{1 + \frac{\delta\eta_3}{[1+(\delta\eta_3)^2]}\right\} \tag{1}$$

The resistance of the nonlinear spring was so selected that it is different in tension and compression when $\delta \neq 0$. This selected resistance with nonzero δ makes the resulting bifurcation path in the x_3 direction asymmetric. The nonlinear relation between force and displacement of the third spring was selected as a matter of preference within the conditions just stated.

The nondimensional equilibrium equations in each direction of the coordinates can be expressed as

$$K_1 = (\chi_1 - \beta)\left(2 - \frac{\ell_1}{\hat{\ell}_1} - \frac{\ell_2}{\hat{\ell}_2}\right) - pf_1 = 0 \tag{2a}$$

$$K_2 = (\chi_2 - 1)\left(1 - \frac{\ell_1}{\hat{\ell}_1}\right) + (\chi_2 + 1)\left(1 - \frac{\ell_2}{\hat{\ell}_2}\right) - pf_2 = 0 \tag{2b}$$

$$K_3 = \chi_3\left(2 - \frac{\ell_1}{\hat{\ell}_1} - \frac{\ell_2}{\hat{\ell}_2}\right) + \gamma(\chi_3 - \chi_3^0) \times \left\{1 + \frac{\delta(\chi_3 - \chi_3^0)}{[1 + \delta^2(\chi_3 - \chi_3^0)^2]}\right\} - pf_3 = 0 \tag{2c}$$

where

$$\ell_1 = [(\chi_1^0 - \beta)^2 + (\chi_2^0 - 1)^2 + (\chi_3^0)^2]^{0.5}$$

$$\hat{\ell}_1 = [(\chi_1 - \beta)^2 + (\chi_2 - 1)^2 + (\chi_3)^2]^{0.5}$$

$$\ell_2 = [(\chi_1^0 - \beta)^2 + (\chi_2^0 + 1)^2 + (\chi_3^0)^2]^{0.5}$$

$$\hat{\ell}_2 = [(\chi_1 - \beta)^2 + (\chi_2 + 1)^2 + (\chi_3)^2]^{0.5}$$

The magnitudes and dimensions of elements of the loading pattern vector f_i (i = 1-3) are selected so that f appearing in the definition of p becomes a scalar representing loading intensity. The governing equilibrium equations of the perfect model can be obtained by setting $\chi_i^0 = 0$ (i = 1-3) in ℓ_i appearing in Eqs. (2).

Basic Behavior of the Perfect Model

The classification of a critical point of a system, perfect or imperfect, can be investigated through its tangential stiffness matrix. The elements of the tangential stiffness matrix of the model are given in the Appendix.

Considering the case that only a vertical force is applied, Eqs. (2b) and (2c) are satisfied for a perfect model when $\chi_2 = \chi_3 = 0$. The main path of the perfect model then can be expressed as

$$p = 2(\chi_1 - \beta)\left\{1 - \frac{(1+\beta^2)^{0.5}}{[(\chi_1 - \beta)^2 + 1]^{0.5}}\right\}, \qquad \chi_2 = \chi_3 = 0 \tag{3}$$

The main path of the perfect model is a function of β and independent of γ and δ. The eigenvalues and corresponding unit eigenvectors of the tangential stiffness matrix along the main path are given as

$$\bar{\lambda}_1 = 2\left\{1 - \frac{(1+\beta^2)^{0.5}}{[(\chi_1 - \beta)^2 + 1]^{1.5}}\right\} \tag{4a}$$

$$\bar{e}_1 = <1\ 0\ 0>^T \tag{4b}$$

$$\bar{\lambda}_2 = 2\left\{1 - (\chi_1 - \beta)^2 \frac{(1+\beta^2)^{0.5}}{[(\chi_1 - \beta)^2 + 1]^{1.5}}\right\} \tag{4c}$$

$$\bar{e}_2 = <0\ 1\ 0>^T \tag{4d}$$

$$\bar{\lambda}_3 = 2\left\{1 - \frac{(1+\beta^2)^{0.5}}{[(\chi_1 - \beta)^2 + 1]^{0.5}}\right\} + \gamma \tag{4e}$$

$$\bar{e}_3 = <0\ 0\ 1>^T \tag{4f}$$

The zero value of the first eigenvalue gives stationary points since $\bar{e}_1 \cdot f \neq 0$, whereas those of the other two give bifurcation points since $\bar{e}_2 \cdot f = \bar{e}_3 \cdot f = 0$, with bifurcation paths in the x_2 and x_3 directions, respectively, as can be seen by the corresponding eigenvectors.[9] It is noted that all eigenvalues are functions of β but independent of δ, and, in addition, that $\bar{\lambda}_3$ is a function of γ as well.

The nondimensional positions and loading intensities of the stationary points on the main path can be obtained by equating Eq. (4a) to zero and substituting the obtained $\bar{\chi}_1^{cr}$ into Eq. (3), resulting in

$$\bar{\chi}_1^{cr} = \beta \pm [(1+\beta^2)^{1/3} - 1]^{0.5}, \qquad \bar{\chi}_2^{cr} = \bar{\chi}_3^{cr} = 0$$

$$\bar{p}^{cr} = \pm 2[(1+\beta^2)^{1/3} - 1]^{1.5} \tag{5}$$

The model has bifurcation paths in the x_2 direction on the main path when $\bar{\lambda}_2$ of Eq. (4c) is zero. Equating Eq. (4c) to zero yields a cubic equation in terms of $1/[(\chi_1 - \beta)^2 + 1]^{0.5}$ as

$$1 - \frac{(1+\beta^2)^{0.5}}{[(\chi_1 - \beta)^2 + 1]^{0.5}} + \frac{(1+\beta^2)^{0.5}}{[(\chi_1 - \beta)^2 + 1]^{1.5}} = 0 \tag{6}$$

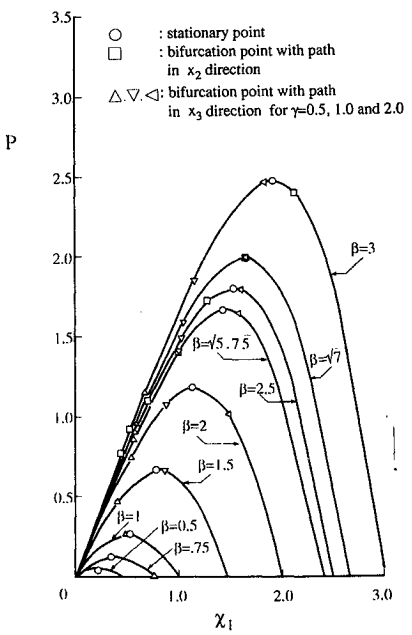

Fig. 2 Main equilibrium paths.

It has positive real roots of χ_1 only if $\beta^2 \geq 5.75$. When $\beta^2 = 5.75$, the model has two bifurcation points that exist before the first and after the second stationary points of the main equilibrium path, respectively. The first bifurcation point of these two is shown in Fig. 2 by the symbol □ on the path ($\beta = \sqrt{5.75}$), selecting the nondimensional loading intensity and the nondimensional displaced position χ_1 for vertical and horizontal axes, respectively. For a larger β, each bifurcation point separates into two, and hence the model has four bifurcation points. The first two of them are also shown by the symbol □ in Fig. 2 on the paths where $\beta > \sqrt{5.75}$.

The nondimensional positions and loading intensities of the bifurcation points corresponding to the bifurcation paths in the x_3 direction can be obtained by equating Eq. (4e) to zero and substituting the obtained $\bar{\chi}_1^{cr}$ into Eq. (3) leading to

$$\bar{\chi}_1^{cr} = \beta \pm \frac{[4\beta^2 - 4\gamma - \gamma^2]^{0.5}}{(2+\gamma)}, \qquad \bar{\chi}_2^{cr} = \bar{\chi}_3^{cr} = 0$$

$$\bar{p}^{cr} = \pm\gamma \frac{[4\beta^2 - 4\gamma - \gamma^2]^{0.5}}{(2+\gamma)} \tag{7}$$

These bifurcation points exist when $\bar{\chi}_1^{cr}$ and $\bar{p}_1^{cr}$ of Eq. (7) are real, i.e., the term inside the bracket is positive or equal to zero. This condition is satisfied for a given β if $\gamma \leq 2[(1+\beta^2)^{0.5} - 1]$, and for a given γ if $\beta^2 \geq \gamma + 0.25\gamma^2$. When the equality condition holds, a bifurcation point in the x_3 direction appears. When the inequality condition holds, the point separates into two bifurcation points. The first bifurcation point coincides with the first stationary point when $\beta = [(1+\gamma/2)^3 - 1]^{0.5}$. Different locations of these bifurcation points for different β and γ are shown in Fig. 2. If desired, the stationary and the two bifurcation points with bifurcation paths in the x_2 and x_3 directions can be made to coincide with each other by proper selection of β and γ. This state can be achieved when $\beta = \sqrt{7}$ and $\gamma = 2$ as can be seen in Fig. 2.

Noting that the tangential stiffness matrix of the perfect model is always diagonal along the main path, the initial slope of the bifurcation paths in the x_2 and x_3 directions depends on the values of $\partial^2\bar{K}_2/\partial\chi_2^2$ and $\partial^2\bar{K}_3/\partial\chi_3^2$, respectively. Noting $f_2 = f_3 = 0$, this is valid as long as the bifurcation point is a distinct critical point and $\partial^2\bar{K}_2/\partial\chi_1^2$ and $\partial^2\bar{K}_3/\partial\chi_1^2$ are nonzero, respectively.[9] The values of $\partial^2\bar{K}_2/\partial\chi_2^2$ and $\partial^2\bar{K}_3/\partial\chi_3^2$ of the perfect model are expressed as

$$\frac{\partial^2\bar{K}_2}{\partial\chi_2^2} = 3(1+\beta^2)^{0.5}\left[\frac{(\chi_2-1)}{\hat{\ell}_1^3} + \frac{(\chi_2+1)}{\hat{\ell}_2^3}\right] + 3(1+\beta^2)^{0.5}\left[\frac{(\chi_2-1)^3}{\hat{\ell}_1^5} + \frac{(\chi_2+1)^3}{\hat{\ell}_2^5}\right] \tag{8}$$

$$\frac{\partial^2\bar{K}_2}{\partial\chi_2^2} = 3(1+\beta^2)^{0.5}\chi_3\left[\frac{1}{\hat{\ell}_1^3} + \frac{1}{\hat{\ell}_2^3}\right] + 3(1+\beta^2)^{0.5}\chi_3^3\left[\frac{1}{\hat{\ell}_1^5} + \frac{1}{\hat{\ell}_2^5}\right] + 2\gamma\delta\left\{\frac{1}{[1+(\delta\chi_3)^2]} - \frac{5(\delta\chi_3)^2}{[1+(\delta\chi_3)^2]^2} + \frac{4(\delta\chi_3)^4}{[1+(\delta\chi_3)^2]^3}\right\} \tag{9}$$

Noting that $\chi_2 = 0$ and $\hat{\ell}_1 = \hat{\ell}_2$ on the main equilibrium path, $\partial^2\bar{K}_2/\partial\chi_2^2$ is equal to zero for any value of β, which shows that the bifurcation path in the x_2 direction has zero initial slope.[9] Since Eqs. (2) are even functions of χ_2 when $f_2 = f_3 = 0$, the bifurcation path is symmetric. On the other hand, substituting Eq. (7) into $\partial^2\bar{K}_3/\partial\chi_3^2$ yields $2\gamma\delta$ for any value of β, which shows that the bifurcation path in the x_3 direction is generally asymmetric when $\delta \neq 0$. For a given γ, the initial slope can be varied by changing δ.[9] However, even if $\delta \neq 0$, the initial slope of the bifurcation path becomes equal to zero, when the bifurcation point coincides with the stationary point of the main equilibrium path.[9] Since Eqs. (2) are not even functions of χ_3 for nonzero δ, the bifurcation path in the x_3 direction is asymmetric with zero initial slope. This definition is different than that of Thompson and Hunt.[1] When the initial slope is zero, they defined the bifurcation as a symmetric bifurcation.

Optimization of Initial Imperfection for the Lowest Carrying Capacity

The optimization for the lowest carrying capacity of the model under a given norm of imperfections with the application of a vertical load is formulated as

$$\text{minimize } p^* \tag{10a}$$

subject to

$$K_i[\chi_i^*, (\chi_i^0)^*] - p^* f_i = 0, \qquad \lambda_s = 0$$

$$[(\chi_1^0)^*]^2 + [(\chi_2^0)^*]^2 + [(\chi_3^0)^*]^2 = r^2 \tag{10b}$$

The unknowns of this optimization problem are $(\chi_i^0)^*$, χ_i^*, and p^*. Noting that all constraints are equality constraints, this optimization can be solved by the method of Lagrange multipliers.

For explanatory purposes of the preceding optimization for a general system and for simplicity, representative equilibrium paths of a two-degree-of-freedom perfect system and optimum imperfect system for a given norm of imperfections are shown in Fig. 3 by solid and dashed lines, respectively. The critical points of the perfect system are marked by open dots, whereas those of the optimum imperfect systems are marked by solid dots. The same symbols for the critical points are used in the subsequent figures. The chain line indicates the locus of the optimum first critical points of all imperfect systems under a given norm of imperfections. The optimum imperfect systems have their first critical points on the stationary points of this chain line. These stationary points are marked by points a to d. The initial positions of the imperfect system that lead to the optimum solutions a to d are marked by a_i to d_i, respectively.

For all the numerical examples, the equilibrium paths of the perfect model were found by solving Eqs. (2) with $\chi_i^0 = 0$ ($i = 1$-3). Parts of them are plotted by solid lines in the subsequent figures. Their critical points on the main paths were found by solving Eqs. (5-7), whereas those on the bifurcation paths were found by singularity of their tangential stiffness matrices. If it is required, the equilibrium paths of optimum imperfect models can be obtained by solving Eqs. (2) with the obtained critical modes of imperfection $(\chi_i^0)^*$ by the optimization of Eqs. (10), and parts of them are plotted by dashed lines in the subsequent figures.

Numerical Studies

General Instability Behavior

A numerical study was made on various values of β, γ, and δ. All modes of the bifurcation and main paths at each critical point were used to obtain initial guess solutions for the initial imperfection and for the optimum position for optimization, detail of which is given in the previous work by the authors.[8]

The equilibrium paths of perfect and optimum imperfect models are plotted using the norm of nondimensional coordinates (displacements) and the nondimensional loading intensity as horizontal and vertical axes, respectively. This axis system was also employed in the previous work of the authors[8] as a representative two-dimensional presentation of the equilibrium paths in $(n+1)$ dimensional space. The loci of the global optimum points for imperfect systems are plotted by chain lines. If preferable for explanatory purposes, the loci of other optimum critical points are plotted by thinner chain lines, which are obtained if necessary by replacing λ_s of Eq. (10b) to an appropriate λ_i ($i = 1$-3) of Eq. (4).

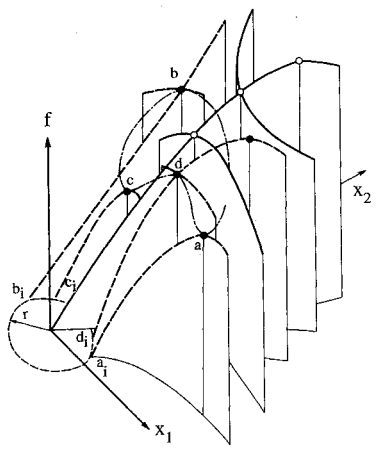

Fig. 3 Equilibrium paths of two-degree-of-freedom perfect and optimum imperfect systems.

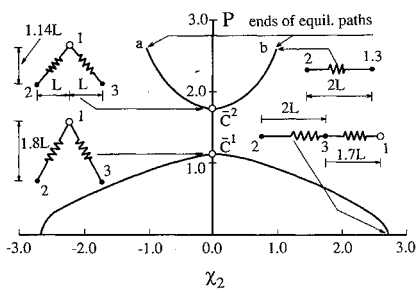

Fig. 4 Bifurcation path in x_2 direction.

The solutions of the optimization formulated by Eqs. (10) are presented in the subsequent figures as the relation between the nondimensional optimum loading intensity p^* vs the norm of imperfection r. The solid and dashed lines indicate that solutions are stationary and bifurcation points, respectively.

The use of the mode of a symmetric bifurcation path as the initial guess solution for initial imperfection and for the optimum position yields two mirror symmetric optimum solutions, i.e., two solutions with the same loading intensities and the same positions but with opposite signs for each component of the latter. In the relation between p^* and r, these two optimum solutions coincide and are marked by "Sym" in the subsequent figures. Using the mode of an asymmetric path yields two nonmirror symmetric solutions. Different optimum loading intensities indicate that they correspond to each side of the path emanating from the bifurcation point. In the subsequent figures, these two solutions are marked by "Asym_n" and "Asym_p" representing the negative and positive sides of the asymmetric path in the x_3 direction, respectively. However, when $\delta = 0$, which gives a symmetric path, the two coinciding solutions are marked by "Asym_s." Using the mode of the main path generally yields two solutions corresponding to a smaller and a larger β with different optimum loading intensities. They are marked in the subsequent figures by "Main_s" and "Main_ℓ" representing a smaller and a larger β, respectively. In these cases, the imperfect models have the same shapes as the perfect one, but with different heights.

Example 1

As the first numerical example, the values of β and γ were selected to be 2.5 and 4.0, respectively. The latter was selected to make the model bifurcating only in the x_2 direction. The aim of this example is to show the possibility that a continuous equilibrium path terminates at a point in the $(n+1)$ dimensional space and jumps to another point even when the geometrical change of a system is continuous. If this happens, special care is necessary to estimate an initial guess solution in obtaining equilibrium solutions by an iterative process such as the Newton-Raphson method.

The main equilibrium path of this three-spring model is presented in Fig. 2. The bifurcation paths in the x_2 direction for the model with $\beta = 2.5$ are plotted in Fig. 4 using p and χ_2 as the vertical and horizontal axes, respectively. Two bifurcation paths emanate at points $\bar{C}^1$ and $\bar{C}^2$ from the main path, which coincides with the vertical axis. Figure 4 shows only the paths with positive loading intensity, which is half of all the bifurcation paths. The other half is mirror symmetric with respect to the horizontal axis. Figure 4 shows that the bifurcation path emanating from $\bar{C}^2$ terminates at points marked by a and b. At these states, the connecting node of the springs coincides with one of the supporting nodes. To maintain the equilibrium when this node moves below the horizontal line connecting the two supporting nodes, the resulting force of the linear springs changes direction. This makes the bifurcation paths from both a and b jump to the corresponding points on the other mirror-symmetric side of the same paths.

Example 2

As the second numerical example, the model with $\beta = 2$, $\gamma = 1$, and $\delta = 2$ was selected. The main aim of this example is to show that, depending on which side of an asymmetric path is used, optimum solutions of an imperfect system may converge to different critical points of the perfect system when norms of imperfections r approaches zero. Another aim is to show a possibility that the locus of optimum solutions is not necessarily continuous; it terminates at a point and then jumps to a point away in the $(n+1)$ dimensional space even when the norm of initial imperfections is changed continuously.

The perfect model has one bifurcation point $\bar{C}^1$ with a bifurcation path in the x_3 direction before the first stationary point $\bar{C}^2$ as shown in the right-hand side of Fig. 5. Figure 6 is a replot of the right-hand side of Fig. 5 for explanatory purposes, changing the horizontal axis into χ_3. The asymmetric bifurcation path of the perfect model toward the positive direction of χ_3 has a stationary point marked by $\bar{C}^{11}$, while that toward the negative direction has two stationary points marked by $\bar{C}^{12}$ and $\bar{C}^{13}$. Using the same mode of the bifurcation path from $\bar{C}^1$ but with opposite signs for initial guess solution, two optimum solutions were obtained, for which the p^* vs r relations are plotted with the marks Asym_n and Asym_p on the left-hand side of Fig. 5.

The optimum solutions of an imperfect model using the mode of the bifurcation path toward positive χ_3 direction converge to $\bar{C}^{11}$ when r approaches zero, as can be seen in the right-hand sides of Figs. 5 and 6. For all values of r, the optimum solutions are stationary points. On the other hand, the optimum solutions for the mode in the opposite direction converge to $\bar{C}^1$ when r approaches zero, as can be seen in the right- and left-hand sides of Figs. 5 and 6, respectively. For a smaller r, this equilibrium path of the optimum imperfect model has three stationary points corresponding to $\bar{C}^1$, $\bar{C}^{12}$, and $\bar{C}^{13}$, respectively, as can be seen in the left-hand side of Fig. 6 for $r = 0.08$. For a larger r, the two stationary points corresponding to $\bar{C}^1$ and $\bar{C}^{12}$ approach each other and coincide at $r = 0.14$, marked by a in Figs. 5 and 6. At this state, the two stationary points become a saddle point. Then, this saddle

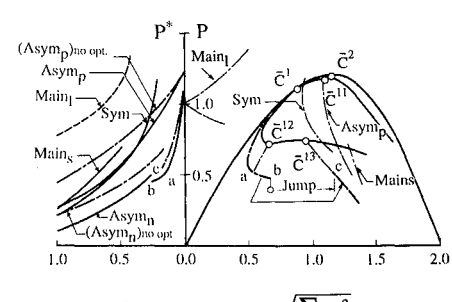

Fig. 5 Equilibrium paths and p^* vs r of perfect model with loci of optimum points.

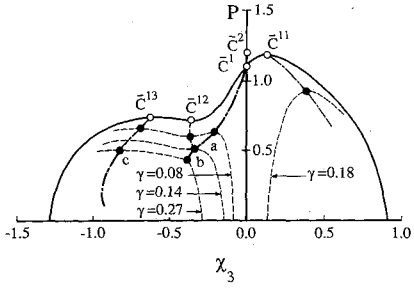

Fig. 6 Equilibrium paths of perfect and optimum imperfect models.

point disappears when r reaches 0.27 marked by b in the same figures. This behavior is shown in the left-hand side of Fig. 6 on the equilibrium paths of the optimum imperfect models with $r=0.08$, 0.14, and 0.27, respectively.

Because of this disappearance of the merged point corresponding to $\bar{C}^1$ and $\bar{C}^{12}$, the locus of the optimum solutions starting from $\bar{C}^1$ jumps from b to c at $r=0.27$. From point c onward, the optimum solutions become the points corresponding to $\bar{C}^{13}$, which are stationary points. For a complex structural system, detecting a similar jump itself would be a difficult task. Nevertheless, when continuous optimum solutions fail to converge all of a sudden, attention has to be paid to this sort of jump as a possible cause. Similar to the first example, to obtain optimum solutions after this sort of jump, special care is necessary for the selection of an initial guess solution. The estimation of an initial guess solution can be made by tracing equilibrium paths of optimum structural systems and observing the behavior of singular points on the paths with the norm at which the continuous optimum solutions cease to exist and at the norms nearby such as shown by dashed lines in the left-hand side of Fig. 6.

The fact that the optimum solutions using both sides of the asymmetric bifurcation path of this model for an initial guess solution converge to different critical points when r approaches zero indicates the existence of a discontinuity of the locus of the optimum solutions at the first critical point at $\chi_3^c=0$. The optimum solutions corresponding to the main path mode are expected to have a zero value of χ_3^c. Using both sides of the main path at $\bar{C}^1$ as the modes for an initial guess solution yields no optimum solution for a small value of r. This seems to be due to the previously discussed discontinuity at the first critical point at $\chi_3^c=0$. The formulation of Eq. (10) requires an optimum solution to be a stationary point of the locus of the first critical point as explained for the locus in Fig. 2. They start to exist for a certain value of r when that discontinuity disappears. This happens when the asymmetric bifurcation point becomes the second critical point.

Using the mode of the main path for an initial guess solution, the optimum solution, for which the imperfect model has a smaller β, starts to exist at $r\approx 0.46$, i.e., β of the imperfect model ≈ 1.54. This occurs because the asymmetric bifurcation point $\bar{C}^1$ approaches the first stationary point $\bar{C}^2$ with decreasing β. It coincides with the stationary point when $r\approx 0.46$ and then becomes the second critical point for a larger r. Since the stationary point becomes the first critical point for $r>0.46$, the optimization using the mode of the stationary point, i.e., the mode of the main path, converges to optimum solutions. On the other hand, the optimum solution, for which the imperfect model has a larger β, is expected to appear at $r\approx 0.40$, i.e., β of the imperfect model $=\sqrt{5.75}$ because of the sudden appearance of a critical point before the bifurcation point $\bar{C}^1$ with a bifurcation path in the x_2 direction. This makes the asymmetric bifurcation point become the second critical point. This critical point, which appears by the change of geometry due to initial imperfection at the loading free initial state, is defined in this paper as a "hidden" critical point. To obtain the optimum solutions corresponding to this hidden critical point, the loading intensity and the mode of the eigenvector of this critical point need to be used to obtain an initial guess solution. More details of this hidden critical point are given later in the fourth example.

Numerical results show that the optimum solutions using the mode of this hidden critical point for an initial guess solution appear not from $r\approx 0.40$ but from $r\approx 0.184$. The presence of optimum solutions for r smaller than 0.40 is due to the difference of β at which the hidden critical point appears for imperfect systems when the symmetrically arranged springs 1 and 2 are on an inclined plane compared to $\beta=\sqrt{5.75}$ of the perfect system for which they are on the vertical plane defined by the x_1-x_2 coordinates. The curve marked by Sym in the left-hand side of Fig. 5 is made up of the optimum solutions corresponding to the bifurcation path of this hidden bifurcation point.

Reduction of Carrying Capacity by Optimization

The current practice of studying the effect of initial imperfection in reducing carrying capacity employs a fixed mode of initial imperfection rather than performing optimization of the mode as proposed by the authors.[8] To check the difference with and without optimization, the carrying capacities of the third example were also evaluated by fixing the mode of initial imperfection to the mode at the first critical point with an asymmetric bifurcation path. The results are plotted by the chain lines in the left-hand side of Fig. 5. It shows that the current practice without optimization may overestimate the carrying capacity of an imperfect system.

Example 3

The main aim of this example is a preparation to explain in the fourth example one possible cause of extremely high imperfection sensitivity. Another aim is to show the possibility that critical points present in a perfect system may disappear when initial imperfection is present. This disappearance of critical points causes a jump of location of optimum solutions even for continuous change of norms of imperfections as observed in the second example.

The value of β was selected to be 2.425. This value is slightly larger than $\sqrt{5.75}$, which is the minimum β for the model to exhibit a bifurcation path in the x_2 direction before the first

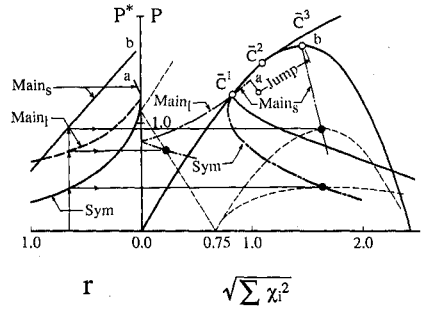

Fig. 7 Equilibrium paths and p^* vs r of perfect and optimum imperfect models with loci of optimum points.

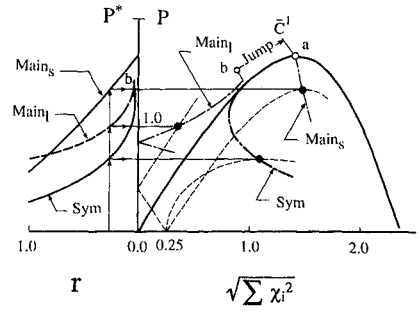

Fig. 8 Equilibrium paths and p^* vs r of perfect and optimum imperfect models with loci of optimum points.

stationary point is reached on the main path. The value of γ was selected to be 4.0 to make the model bifurcate only in the x_2 direction.

The perfect model has symmetric bifurcation paths from two bifurcation points $\bar{C}^1$ and $\bar{C}^2$ as shown in the right-hand side of Fig. 7. The relations of p^* vs r are plotted on the left-hand side of the same figure. Using the modes of the main and the bifurcation path at $\bar{C}^1$ for each initial guess solution, four solutions were obtained, including two identical solutions when plotted in Fig. 7. The solutions using the main path mode from $\bar{C}^1$, which gives a smaller β, i.e., Main_s, are present from $\bar{C}^1$ to a and then jump to b where β of the corresponding imperfect model is equal to $\sqrt{5.75}$, which takes place when $r \approx 0.027$. The reason for this jump is that, at this state and at a larger r, the two bifurcation points $\bar{C}^1$ and $\bar{C}^2$ disappear, and hence the next critical point on the same equilibrium path, which is the stationary point $\bar{C}^3$, becomes the first critical point. For explanatory purposes, the equilibrium paths of the optimum imperfect models for $r = 0.70$ are plotted in the right-hand side of Fig. 7.

Example 4

The values of β equal to 2.375 and γ equal to 4.0 were selected. The value of β is slightly smaller than $\sqrt{5.75}$. The perfect model has no bifurcation points before a stationary point $\bar{C}^1$ is reached, as shown in the right-hand side of Fig. 8, due to this selection of β and γ.

The aim of this example is to show the possibility of having a solution for which the critical mode of imperfection is entirely different from any modes of the critical points of a perfect system. A related but more important aim is to show that the existence of this solution with entirely different modes could be one of the causes of high imperfection sensitivity. This solution exists when norms of initial imperfections exceed a certain value. At this state, critical points equivalent to $\bar{C}^1$ and $\bar{C}^2$ of the third example appear.

Four optimum solutions were obtained, for which the p^* vs r relations are plotted at the left-hand side of Fig. 8. Two solutions among the four are identical in this plot. The solution using the main path mode, which gives a larger β, i.e., Main_ℓ, is almost identical with those of Main_s for a small value r, but it jumps to b when $r \approx 0.023$. With $r \approx 0.023$, β of the imperfect model becomes equal to $\sqrt{5.75}$. At this state, a new critical point, which is a bifurcation point with the path in the x_2 direction, appears. The appearance of this new critical point is the reason for this jump, which is similar to the jumps observed in the second and third examples. The appearance of the bifurcation path in, the x_2 direction indicates that there must be an optimum solution corresponding to its mode. Numerical results show that the solutions using the mode of this bifurcation path for initial guess solution appear starting not from $r \approx 0.023$ but from $r \approx 0.004$. The presence of optimum solutions for r smaller than 0.023 is due to the same reason explained in the second example. For explanatory purposes, three equilibrium paths of optimum imperfect models are plotted in the right-hand side of Fig. 8 for $r = 0.25$.

Observation in Examples 3 and 4

The results of the two examples presented in Figs. 7 and 8 show that there are cases where the behavior of an imperfect system can be quite different from that of the perfect one even for a very small norm of imperfections. When hidden critical points exist, the system could be very sensitive to imperfection. The carrying capacities of the models for both examples are not much different for the same given norm of imperfections. The reduction from the loading intensity of the first critical point of the perfect model, however, is much larger in the fourth example. This larger reduction and hence higher imperfection sensitivity is due to the presence of the hidden bifurcation points.

These examples show that, to study the imperfection sensitivity of a system, tracing the equilibrium paths of the perfect system and performing eigenvalue analysis are important and necessary. The latter is necessary to detect all existing and hidden critical points and to predict the possibility of the disappearance of existing and the appearance of nonexisting critical points. The possibility of both of them is illustrated in Fig. 9 for the third and fourth examples. In Fig. 9, the first and second eigenvalue curves evaluated at the displaced positions of the main paths are plotted together with the main equilibrium paths by solid and dashed lines, respectively. The existing critical points on the main path are marked by open dots.

The possibility of the appearance and disappearance of the critical points with bifurcation paths in the x_2 direction can be detected by observing the curves of $\bar{\lambda}_2$. If it is not equal to but close to zero, as can be seen for the fourth example, the possibility of the appearance of hidden critical points is present. On the other hand, the possibility of the disappearance of critical points can be detected by observing $\bar{\lambda}_2$ in the vicinity of its zero value. If two zero values are closely located on the same eigenvalue curve, as those of $\bar{\lambda}_2$ for the third example, the possibility of the disappearance of these critical points exists even for a small value of the norm of imperfections.

To obtain the equilibrium paths emanating from the hidden critical points of an imperfect system, the loading intenstity and the mode of the eigenvector at the state, where the eigenvalue close to zero is the minimum, are to be used to estimate initial guess solution.

Examples 5 to 7

Three numerical examples were analyzed with $\beta = \sqrt{5.75}$, $\gamma = 1.2$, and $\delta = 0$, 1, and 8, respectively. The aim of these examples is to show the relation between the shape of equilibrium paths and the mode to be used for an initial guess solution to obtain the critical mode of imperfections. The equilibrium paths of the perfect model are shown on the left-hand sides of Fig. 10 for each value of δ, respectively. The main paths of all of them exhibit two bifurcation points, $\bar{C}^1$ and $\bar{C}^2$, with the paths in the x_2 and x_3 directions, respectively, before the first stationary point $\bar{C}^3$ is reached. Because of the selected value of β, two bifurcation paths emanate from the distinct bifurcation point $\bar{C}^1$. They correspond to those emanating from $\bar{C}^1$ and $\bar{C}^2$ of Fig. 4. The initial slope of the bifurcation path in the x_3 direction can be varied by giving a different value of δ. This slope becomes zero when $\delta = 0$. On the other hand, the symmetric bifurcation path in the x_2 direction and the main path remain the same for any value of δ.

The p^* vs r relations using the modes of all bifurcation paths at $\bar{C}^1$ and $\bar{C}^2$ and the main path at $\bar{C}^3$ for an initial guess solution are plotted on the right-hand side of Fig. 10 for $\delta = 0$, 1, and 8, respectively. When $\delta = 0$, using the main path mode yields two different solutions, Main_ℓ, starting from $\bar{C}^1$, and Main_s from $\bar{C}^2$. The latter is due to the disappearance of the symmetric bifurcation point $\bar{C}^1$ since β becomes less than $\sqrt{5.75}$, hence $\bar{C}^2$ becomes the first symmetric critical point. Using those of the symmetric bifurcation paths in the x_2 and x_3 directions yields two mirror symmetric solutions for each path. On the other hand, for nonzero δ, only the mode of

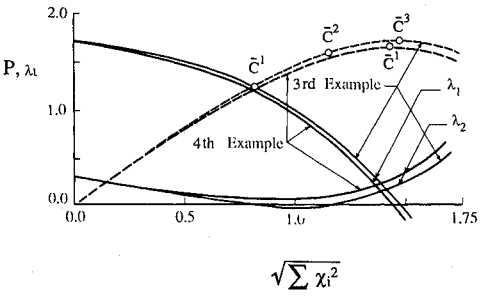

Fig. 9 Eigenvalue curves and main equilibrium paths.

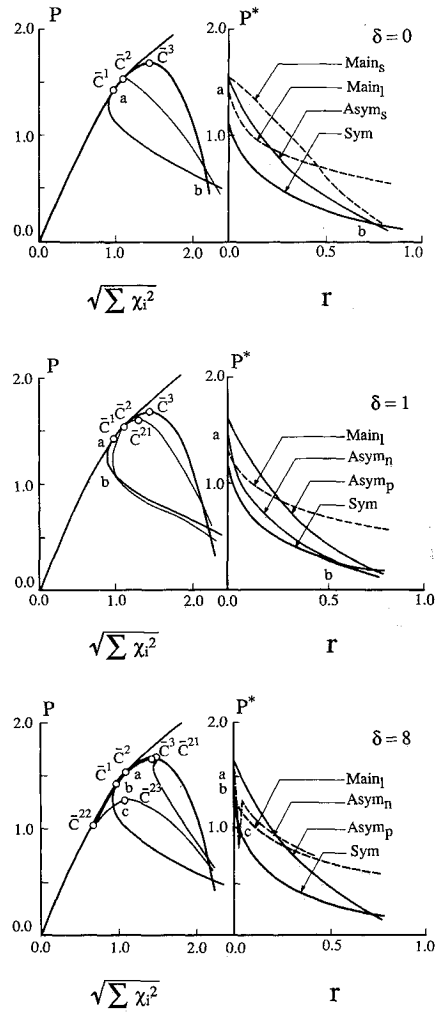

Fig. 10 Equilibrium paths of perfect model and p^* vs r relations.

main path that gives a larger β has a solution. The reason for this is that the asymmetric bifurcation point remains to be the second critical point for a larger β, but it becomes the first critical point for a smaller β because of the disappearance of $\bar{C}^1$ and hence has no optimum solution as explained in the second example. Using the mode of the asymmetric path yields two different optimum solutions and that of the symmetric path yields two mirror symmetric solutions. The optimum solutions using the asymmetric path do not converge to the same critical point when r approaches zero for the same reason as the second example.

To give a better illustration of the relation between the shape of equilibrium paths of the perfect model and the critical mode of imperfections, the crossing points of the curves in the p^* vs displacement and r relations of Fig. 10 are marked by the same lowercase roman letters. The crossing points in these two-dimensional presentations of the equilibrium paths are introduced for explanatory purposes. They are not the real intersecting points of the curves, since they are the curves in $(n+1)$-dimensional space.

Shape of Equilibrium Paths and Modes for the Initial Guess Solution

The left-hand side of Fig. 10 for $\delta = 0$ shows that the symmetric path from $\bar{C}^1$ is the lowest path for almost the entire range from a($\bar{C}^1$) to b. Comparing the left- and right-hand sides of the figure, an almost similar tendency can be observed. The lowest envelope in the right-hand side of Fig. 10 is that using the mode of the bifurcation path from $\bar{C}^1$ for initial guess solution from a to b.

The lowest path in the left-hand side of Fig. 10 for $\delta = 1$ is the bifurcation path from $\bar{C}^1$ from a($\bar{C}^1$) to b; then it is replaced by the bifurcation paths of the negative side of $\bar{C}^2$ from b to c. From c onward, the main path becomes the lowest path. The right-hand side of the figure shows that the lowest envelope from a($\bar{C}^1$) to b is the solution using the mode of bifurcation path from $\bar{C}^1$; then it is replaced by that using the mode corresponding to the negative side of the bifurcation path from $\bar{C}^2$ from b to c. From c onward, the solution using the mode of the main path becomes the lowest envelope.

The left-hand side of Fig. 10 for $\delta = 8$ shows that the lowest path is that of the bifurcation path from $\bar{C}^1$ for the very small range from a($\bar{C}^1$) to b, which can hardly be seen in the figure; then it is replaced by that of the negative side of $\bar{C}^2$ for the small range from b to c. From c onward, the bifurcation path $\bar{C}^1$ again becomes the lowest path. Similar correlation can be observed in the right-hand side of the figure, where the lowest envelopes from a to b, and from b to c, and then c onward are those using the mode of $\bar{C}^1$, $\bar{C}^2$, and again $\bar{C}^1$ for the initial guess solution, respectively.

It is noted in the seventh example that the critical mode of imperfection and hence imperfection sensitivity are related to the steepness of the corresponding bifurcation path of the perfect model in the load-displacement relation plotted with the proposed axis system. In addition, the critical mode of imperfection may correspond to the bifurcation path from the second critical point of the perfect model even for a small norm of imperfections. This clearly shows that the study of imperfection sensitivity should be made considering not only the first critical point but also other critical points of a perfect model as well.

Conclusions

Although the model used in this numerical study is simple, it can exhibit a variety of behaviors related to elastic instability by changing the three parameters included in the model. It is a reasonably appropriate model to study bifurcation behaviors of a perfect system as well as the related imperfection behavior.

It was found through numerical study that an equilibrium path of a nonlinear system may terminate at a point in the $(n+1)$-dimensional space and jump to another point even when the geometrical change of the system is continuous. Similarly, the locus of optimum solutions of a nonlinear imperfect system, which gives the lowest carrying capacity for a given norm of initial imperfections, may jump from one point to a point away from the previous point even when norms of imperfections are changed continuously. When a solution fails to converge, attention has to be paid to these sorts of jumps as a possible cause. If the aforementioned jumps occur, special care is necessary to estimate an initial guess solution to be used in an iterative process in obtaining equilibrium solutions or optimum solutions.

The numerical study indicates that imperfection sensitivity of a system is related not only to the paths emanating from the first critical point but also to other critical points. The steepnesses of the bifurcation paths from the first and other critical points also influence the imperfection sensitivity of a system. The cases where the modes of bifurcation from other critical points are more critical than that of the first critical point were observed in the last numerical example and the reticulated truss example of the previous work of the authors.[8] The current practice to consider only the first critical point for the study of the effect of imperfection may lead to erroneous results in some cases.

Considering critical points other than the first is important but not sufficient to study imperfection sensitivity. The behavior of imperfect systems is much more complex. The critical points that are not present on the equilibrium paths of a perfect system may appear on those of the imperfect system. This can be detected by checking the behavior of eigenvalues.

If this is the case, the system could become extremely sensitive to imperfection and failure behavior could change abruptly. Such behavior cannot be detected if study is made paying attention only to the modes of the first and a few neighboring critical points of a perfect system.

The numerical study shows that the optimization is necessary, as it may reduce the carrying capacity from the value obtained by using a fixed mode of a path at a critical point as the mode of initial imperfection.

Together with the conclusion made by the authors in the previous work,[8] the last three examples show the relationship between the shape of equilibrium paths of the perfect model and the initial guess solution to obtain the most influential mode of imperfection, defined as the critical mode of imperfection. This relation can help to select an initial guess solution to be tried and hence reduces the computational efforts in the optimization procedure to obtain the critical mode of imperfection and its corresponding load-carrying capacity. The optimization needs to be performed using only, for an initial guess solution, the modes of the paths at critical points of a perfect system that form the lowest and nearby envelopes in the two-dimensional presentation of the load-displacement relation using the loading intensity and the norm of all displacements as the vertical and horizontal axes, respectively, excluding the main equilibrium path from the loading free state up to the first critical point. When the possibility of the appearance of hidden critical points is detected, the loading intensities and the modes of the corresponding hidden critical points are to be used to obtain an initial guess solution.

This study shows that, to study the imperfection sensitivity, the analysis of the perfect system is important and necessary. The analysis should include tracing the main and bifurcation paths and evaluating the eigenvalues to detect existing and hidden critical points.

Appendix: Elements of Tangential Stiffness Matrix

$$\frac{\partial K_1}{\partial \chi_1} = 2 - \left(\frac{\ell_1}{\bar{\ell}_1} + \frac{\ell_2}{\bar{\ell}_2}\right) + (\chi_1 - \beta)^2 \left(\frac{\ell_1}{\bar{\ell}_1^3} + \frac{\ell_2}{\bar{\ell}_2^3}\right) \tag{A1}$$

$$\frac{\partial K_1}{\partial \chi_2} = (\chi_1 - \beta)\left[\frac{\ell_1}{\bar{\ell}_1^3}(\chi_2 - 1) + \frac{\ell_2}{\bar{\ell}_2^3}(\chi_2 + 1)\right] \tag{A2}$$

$$\frac{\partial K_1}{\partial \chi_3} = \chi_3(\chi_1 - \beta)\left(\frac{\ell_1}{\bar{\ell}_1^3} + \frac{\ell_2}{\bar{\ell}_2^3}\right) \tag{A3}$$

$$\frac{\partial K_2}{\partial \chi_2} = 2 - \left(\frac{\ell_1}{\bar{\ell}_1} + \frac{\ell_2}{\bar{\ell}_2}\right) + \left[\frac{\ell_1}{\bar{\ell}_1^3}(\chi_2 - 1)^2 + \frac{\ell_2}{\bar{\ell}_2^3}(\chi_2 + 1)^2\right] \tag{A4}$$

$$\frac{\partial K_2}{\partial \chi_3} = \chi_3\left[\frac{\ell_1}{\bar{\ell}_1^3}(\chi_2 - 1) + \frac{\ell_2}{\bar{\ell}_2^3}(\chi_2 + 1)\right] \tag{A5}$$

$$\frac{\partial K_3}{\partial \chi_3} = 2 - \left(\frac{\ell_1}{\bar{\ell}_1} + \frac{\ell_2}{\bar{\ell}_2}\right) + \chi_3^2\left(\frac{\ell_1}{\bar{\ell}_1^3} + \frac{\ell_2}{\bar{\ell}_2^3}\right) + \gamma\left\{1 + \frac{2\delta(\chi_3 - \chi_3^0)}{[1 + \delta^2(\chi_3 - \chi_3^0)^2]} - \frac{2[\delta(\chi_3 - \chi_3^0)]^3}{[1 + \delta(\chi_3 - \chi_3^0)^2]^2}\right\} \tag{A6}$$

References

[1]Thompson, J. M. T., and Hunt, G. W., *A General Theory of Elastic Stability*, Wiley, London, 1978, Chap. 8.

[2]Thompson, J. M. T., and Hunt, G. W., *Elastic Instability Phenomena*, Wiley, Chichester, England, U.K., 1984, Chaps. 3 and 6.

[3]Ho, D., "Buckling Load of Nonlinear Systems with Multiple Eigenvalues," *International Journal of Solids and Structures*, Vol. 10, No. 11, 1974, pp. 1315–1330.

[4]Huseyin, K., *Multiple Parameter Stability Theory and Its Applications*, Oxford University Press, Oxford, England, U.K., 1986, Chap. 3.

[5]Rosen, A., and Schmit, L. A., "Optimization of Truss Structures Having Local and System Geometric Imperfections," *AIAA Journal*, Vol. 19, No. 5, 1981, pp. 626–633.

[6]Kondoh, K., and Atluri, S. N., "Influence of Local Buckling on Global Instability: Simplified, Large Deformation, Post-Buckling Analyses of Plane Trusses," *Computers and Structures*, Vol. 21, No. 4, 1985, pp. 613–627.

[7]Brendel, B., and Ramm, E., "Linear and Nonlinear Stability Analysis of Cylindrical Shells," *Computers and Structures*, Vol. 12, No. 4, 1980, pp. 549–558.

[8]Nishino, F., and Hartono, W., "Influential Mode of Imperfection on Carrying Capacity of Structures," *Journal of Engineering Mechanics Division*, ASCE, Vol. 115, No. 10, 1989, pp. 2150–2165.

[9]Nishino, F., Hartono, W., Fujiwara, O., and Karasudhi, P., "A Study of the Stability and Behavior at the Critical Point by the Taylor Expansion," *Proceedings of JSCE, Structural Engineering/Earthquake Engineering*, Vol. 4, No. 1, April 1987, pp. 1s–9s.